

Article

Thermodynamic Characteristics Study with Pyrolysis Steam Coupled Multi-Stage Condensers

Yong Bai ¹, Yunfeng Ma ^{1,2,*}, Changjun Ke ^{1,2}, Wang Cheng ¹, Guangyan Guo ¹, Peng Zhao ¹, Can Cao ¹, Lifan Liao ^{1,2}, Xuebo Yang ¹  and Zhongwei Fan ^{1,2}

¹ Aerospace Information Research Institute, Chinese Academy of Sciences, No.9 Deng Zhuang South Road, Beijing 100094, China

² School of Optoelectronics, University of Chinese Academy of Sciences, Yuquan Road No.19, Beijing 100049, China

* Correspondence: mayf100612@aircas.ac.cn

Abstract: A four-stage condensers in series system was adopted to solve the problems of insufficient condensation of high-temperature pyrolysis steam and difficulty in the classification and recovery of pyrolysis oil, where the internal fluids conducted countercurrent convection heat exchange. A steady-state physical and mathematical model of a single condenser was established to clarify the discipline of heat transfer between the internal fluids. Meanwhile, the model of pyrolysis steam coupled multi-stage condensers was proposed with the help of the model compound firstly. A numerical simulation was carried out and the results showed that when the number of condensers in series was four, the heat transfer process of the system reached saturation, and the heat exchange of the cold and hot fluids was completely realized, and it was of little significance to continue to connect more condensers in series for the condensation of pyrolysis steam. To quickly condense the hot fluid, the key was to increase the mass flow rate of the cold fluid in the first-stage condenser. Compared with the experimental values, the calculated values of hot fluid outlet temperature were not higher than 10%, indicating that the model was highly reliable.



Citation: Bai, Y.; Ma, Y.; Ke, C.; Cheng, W.; Guo, G.; Zhao, P.; Cao, C.; Liao, L.; Yang, X.; Fan, Z. Thermodynamic Characteristics

Study with Pyrolysis Steam Coupled Multi-Stage Condensers. *Processes* **2022**, *10*, 2030. <https://doi.org/10.3390/pr10102030>

Received: 8 September 2022

Accepted: 1 October 2022

Published: 8 October 2022

Publisher's Note: MDPI stays neutral with regard to jurisdictional claims in published maps and institutional affiliations.



Copyright: © 2022 by the authors. Licensee MDPI, Basel, Switzerland. This article is an open access article distributed under the terms and conditions of the Creative Commons Attribution (CC BY) license (<https://creativecommons.org/licenses/by/4.0/>).

Keywords: dual tube heat exchanger; heat transfer; model compound; multi-stage condensers; thermodynamic characteristic

1. Introduction

Biomass fast pyrolysis refers to the chemical conversion technology method that in the absence of oxidants (air, oxygen, and water steam) or only limited oxygen, after heating to the certain temperature range, the biomass macromolecular substances (lignin, cellulose, and semi-cellulose) were decomposed into smaller molecular substances (pyrolysis oil, char, and combustible gas) [1–3]. The condensation of high-temperature pyrolysis steam was one of the key parts of the fast pyrolysis technology, which had a great influence on the yield, composition, and quality of pyrolysis oil [4,5]. As one of the pyrolysis steam condensation methods, the staged condensation can not only obtain high-quality products, but also facilitate the recovery of the multi-stage products and obtain a variety of pyrolysis oils with different qualities and applications, whose prospects were excellent and one of the important studies in the field of biomass fast pyrolysis [6–8].

Currently, it is common to use indirect heat exchange condensers (dual tube heat exchangers) as the heat transfer unit of the multi-stage condensers. Many researchers used multi-stage condensers to condense high-temperature pyrolysis steam to achieve the condensation temperature control and product recovery [9,10]. Mati et al. used fractional condensers in series to divide the pyrolysis oil into heavy oil, medium oil, and moisture according to their densities, and initially realized the classification and recovery of products [11]. In the multi-stage condensers system, the condensation temperature was the key parameter. The temperature of the first-stage condenser was usually kept above

80 °C, where water and light carboxylic acid did not condense. The pyrolysis oil collected from this stage condenser had a relatively low water/acid content [12]. Gooty used a three-stage cyclone separation for the heat exchanger, where water or glycol acted as the coolant to circulate in the shell and tube of the heat exchanger to quench the volatile steam flowing inside [13]. The above literature showed that the multi-stage condensation technology can enrich the effective components in the pyrolysis oil and improve its quality. However, many multi-stage condensation temperatures and methods (concurrent and countercurrent, velocity) were different, and it was difficult to provide a theoretical reference for the research and design of the multi-stage condensation apparatus in the fast pyrolysis technology.

However, the composition of the pyrolysis steam was more complicated. If it was directly used in the calculation and numerical simulation of the condensation process, the calculation may be extremely cumbersome [14,15]. Many studies showed that replacing complex compounds with model compounds applied in materials, metallurgy, catalytic reactions, and other fields was one of the important ways to study the different mechanism of the compounds [16–20], that was, each component and its physical and chemical properties was weighted and averaged according to their respective proportions to obtain a certain compound with specific physical and chemical properties, which can simplify the subsequent series of calculations.

The purpose of this paper was to adopt the multi-stage condensation method to determine the most suitable convection heat transfer form of hot and cold fluids, to achieve the efficient heat exchange and product condensation. At the same time, through theoretical calculation methods, the thermodynamic equilibrium of a single condenser and multi-stage condensers was further investigated, with emphasis on its temperature and thermal load regulation characteristics. A pyrolysis steam coupled stage condensers model was established firstly with the help of the concept of the model compound, and the heat transfer differential equations were used to solve the problem to obtain the coupling relationship between all single condensers and the optimal fluid operating parameters of the multi-stage condensation mode. The results provided a new solution for the precise control of the condensation fluids and product collection, which was of great significance for the actual operation and the expansion of the fast pyrolysis production scale.

2. Design

To facilitate staged condensation and recovery of pyrolysis oil, adopting indirect condensing heat exchangers in series was an ideal condensing method. The common dual tube heat exchanger was used as a single condenser unit to realize heat exchange efficiently between high-temperature pyrolysis steam and low-temperature fluid. According to the characteristics of the dual tube heat exchanger, both the inner tube and the outer tube can act as pipelines for hot and cold fluids. Allowing the pyrolysis steam to flow vertically upwards, while the flow direction of the cold fluid (water at different temperatures) was vertical up or down, there were four specific implementation schemes, as shown in Figure 1. The hot fluid condensed through the convective heat exchange with the cold fluid between the inner tube wall, and gradually accumulated to the bottom. The uncondensed part was discharged into the next-stage condenser, and the flow of the cold fluid was driven by a circulating pump.

The outlet temperature, overall heat transfer coefficient, and thermal load of a single condenser in different design schemes were different, which had a greater impact on the condensation effect of pyrolysis steam. Therefore, it was necessary to analyze the thermodynamic characteristics of each scheme and select a suitable direction of cold and hot fluid flow as the design scheme of the condenser.

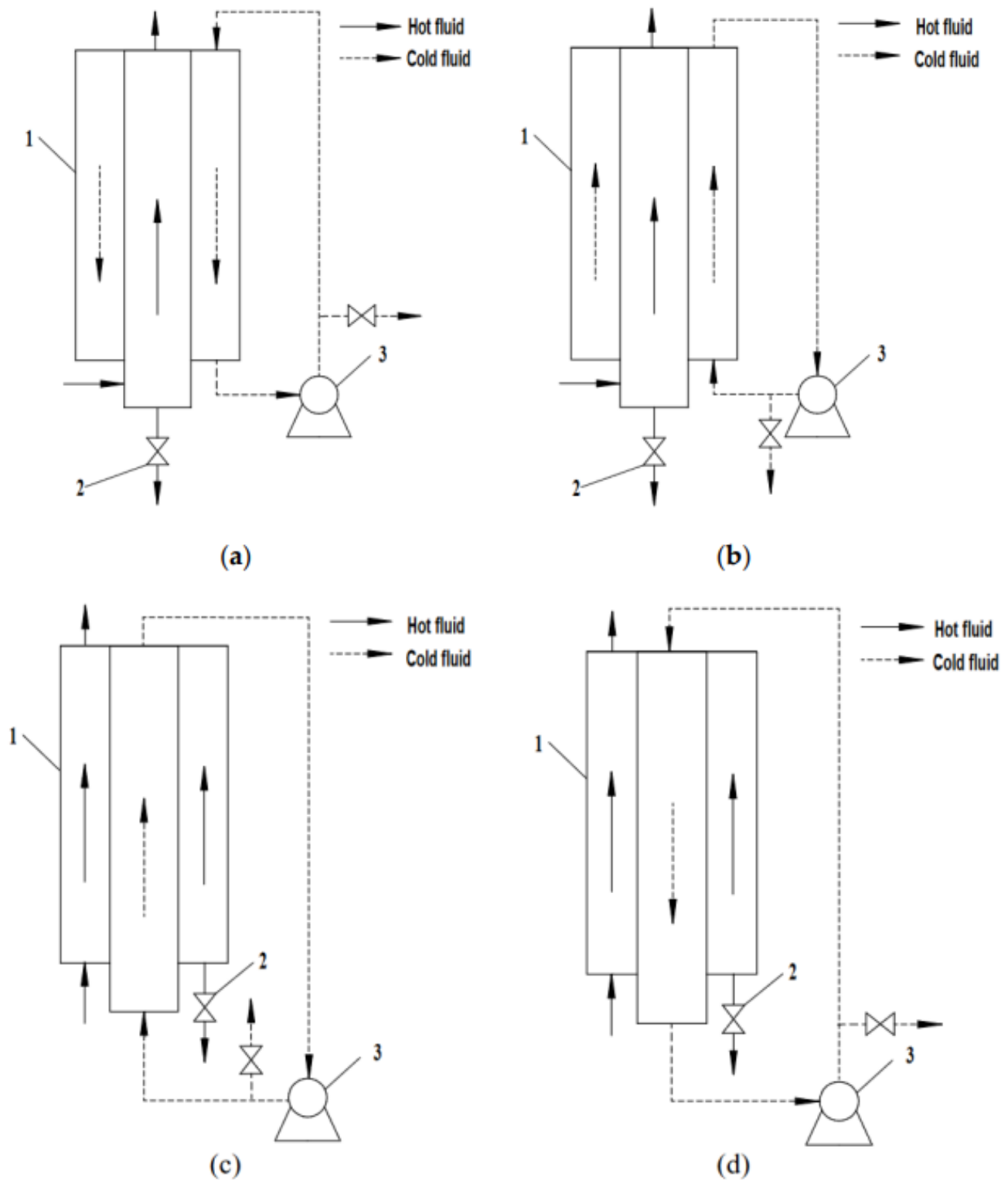


Figure 1. Schemes of the convective heat transfer between the pyrolysis steam and the cold fluid ((a) scheme 1; (b) scheme 2; (c) scheme 3; (d) scheme 4): (1) dual tube heat exchanger; (2) ball valve; (3) circulating pump.

3. Thermodynamic Equilibrium Model Development

3.1. Single Condenser Model

First, four schemes are simplified and a thermodynamic equilibrium model is established to compare and analyze the convective heat transfer schemes. Taking the Scheme 1 as

an example, the structure and control micro-element of the dual tube heat exchanger were established. In Figure 2a, the fluids at different temperatures in the two sides flowed in reverse directions, whose temperatures gradually changed along the flow distance. The main structural parameters are shown in Table 1. Therefore, a distributed parameter differential equation model can be established. Ignoring the temperature of the two fluids in the radial direction, according to the energy conservation relationship of “input-output = accumulation + consumption”, the thermal balance equation in the time interval Δt in the control body of length Δx was established in Figure 2b. The heat exchange parameters involved are shown in Table 2.

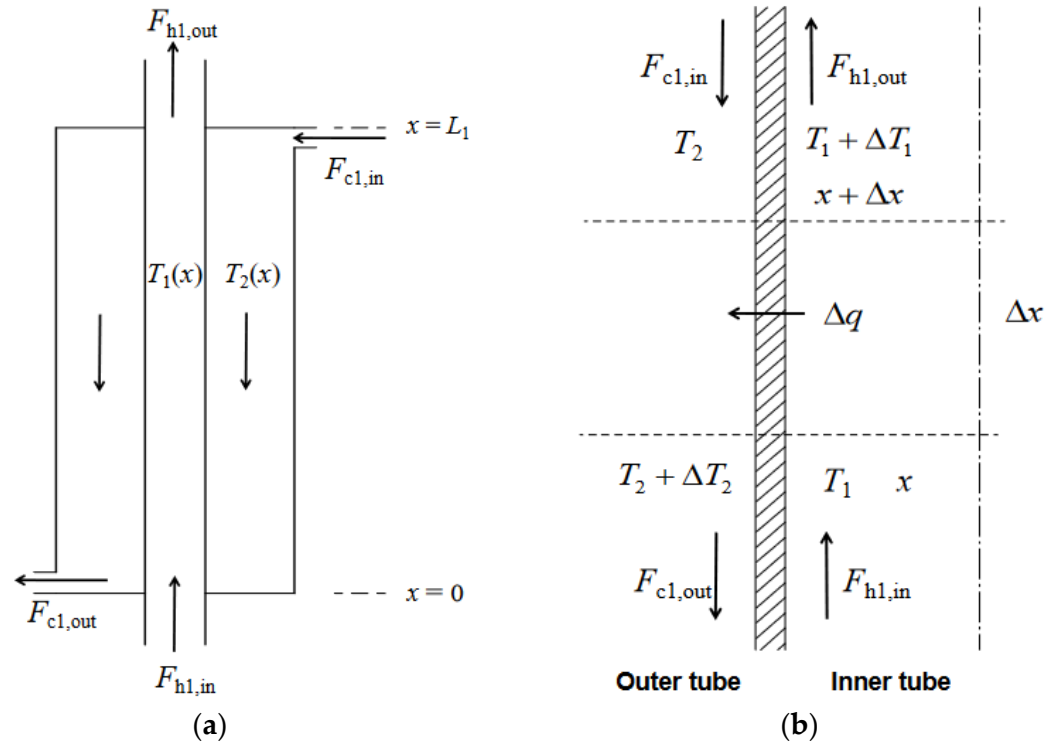


Figure 2. The dual tube heat exchanger: (a) structure; (b) control micro-element.

Table 1. Main Parameters of the Dual Tube Heat Exchanger.

Outer Diameter, mm	Inner Diameter, mm	Thickness, mm	Heat Transfer Height, mm	Effective Heat Transfer Area, m ²
80	40	3	700	0.1

Table 2. Thermal Parameters of the Dual Tube Heat Exchanger.

Parameter	Value
Thermal energy entering the inner tube from the x section	$m_{h1}cp_{h1}T_1\Delta t$
Thermal energy flowing out of the outer tube from the x section	$m_{c1,in}cp_{c1,in}(T_2 + \Delta T_2)\Delta t$
Thermal energy flowing out of the outer tube from the $x + \Delta x$ section	$m_{h1}cp_{h1}(T_1 + \Delta T_1)\Delta t$
Thermal energy entering the inner tube from the $x + \Delta x$ section	$m_{c1,in}cp_{c1,in}T_2\Delta t$
Thermal energy from the inner tube to the outer tube	$\Delta q = K(\pi D\Delta x)(T_1 - T_2)\Delta t$

If the micro-element of the entire tube was calculated, Δq was the internal quantity of the micro-element and did not appear in the balance equation:

$$m_{h1}cp_{h1}T_1\Delta t - m_{c1,in}cp_{c1,in}T_2\Delta t = m_{h1}cp_{h1}(T_1 + \Delta T_1)\Delta t - m_{c1,in}cp_{c1,in}(T_2 + \Delta T_2)\Delta t \quad (1)$$

After eliminating Δt and dividing by Δx , Equation (1) was simplified as Equation (2):

$$\frac{\Delta(m_{h1}cp_{h1}T_1)}{\Delta x} - \frac{\Delta(m_{c1,in}cp_{c1,in}T_2)}{\Delta x} = 0 \quad (2)$$

Taking the limit of $\Delta x \rightarrow 0$, the differential equation was obtained:

$$\frac{d(m_{h1}cp_{h1}T_1)}{dx} - \frac{d(m_{c1,in}cp_{c1,in}T_2)}{dx} = 0 \quad (3)$$

Only when the fluid thermal capacity ($m_{h1}cp_{h1}$ and $m_{c1,in}cp_{c1,in}$) did not change with temperature, Equation (3) can be simplified as Equation (4):

$$m_{h1}cp_{h1} \frac{dT_1}{dx} - m_{c1,in}cp_{c1,in} \frac{dT_2}{dx} = 0 \quad (4)$$

In Equation (4), there was a simple linear relationship between T_1 and T_2 .

If only thermal energy was performed on the micro-elements of the fluid in the inner tube, then Δq appeared in the balance equation:

$$m_{h1}cp_{h1}T_1\Delta t - m_{h1}cp_{h1}(T_1 + \Delta T_1)\Delta t = \Delta q = K(\pi D\Delta x)(T_1 - T_2)\Delta t \quad (5)$$

which can be simplified to obtain:

$$\frac{d(m_{h1}cp_{h1}T_1)}{dx} = -K\pi D(T_1 - T_2) \quad (6)$$

If the fluid thermal capacity $m_{h1}cp_{h1}$ was a constant, Equation (6) can be simplified to a linear ordinary differential equation:

$$m_{h1}cp_{h1} \frac{dT_1}{dx} + K\pi DT_1 = K\pi DT_2 \quad (7)$$

Similarly, the calculation of the fluid in the outer tube can be obtained:

$$-m_{c1,in}cp_{c1,in} \frac{dT_2}{dx} + K\pi DT_2 = K\pi DT_1 \quad (8)$$

Since this model was a one-dimensional ordinary differential equation, the variables T_1 and T_2 to be solved were the functions of the axial distance x , whose boundary conditions were relatively simple. In total, only their values need be specified at the entrances ($x = 0$) of any two positions of the heat exchanger. The known conditions are:

$$x = 0, T_1 = T_{10}; \quad x = L_1, T_2 = T_{20} \quad (9)$$

Because the two boundary conditions were not at the same end point of the solution domain, but at both ends of the solution domain (boundary value problem), the solution process was more difficult than that at the beginning of the solution domain (initial value problem). In the case of unsteady heat transfer, when calculating the thermal balance of the micro-element in the inner tube, it should also be considered that the $\Delta x \times \Delta t$ of the balance domain would appear as the increment ΔT_1 over time in the micro-element, which was:

$$(m_{h1}cp_{h1}T_1)_x\Delta t - (m_{h1}cp_{h1}T_1)_{x+\Delta x}\Delta t = K(\pi D\Delta x)(T_1 - T_2) + S\Delta x \cdot \rho_{h1}cp_{h1}\Delta T_1 \quad (10)$$

After Equation (10) was eliminated, simplified, and its limit was taken, the partial differential equation was obtained:

$$S \frac{\partial(\rho_{h1}cp_{h1}T_1)}{\partial t} + \frac{\partial(m_{h1}cp_{h1}T_1)}{\partial x} = -K\pi D(T_1 - T_2) \quad (11)$$

If the thermal capacities ($m_{h1}, \rho_{h1}, c_{p_{h1}}$) of the fluid were all constants, Equation (11) was simplified as Equation (12):

$$S\rho_{h1}c_{p_{h1}}\frac{\partial T_1}{\partial t} + m_{h1}c_{p_{h1}}\frac{\partial T_1}{\partial x} + K\pi DT_1 = K\pi DT_2 \quad (12)$$

Similarly, the calculation of the fluid in the outer tube can be obtained:

$$S\rho_{c1,in}c_{p_{c1,in}}\frac{\partial T_2}{\partial t} - m_{c1,in}c_{p_{c1,in}}\frac{\partial T_2}{\partial x} + K\pi DT_2 = K\pi DT_1 \quad (13)$$

The boundary conditions to be specified for this countercurrent flow model were:

$$x = 0, T_1 = T_{10}(t); \quad x = L_1, T_2 = T_{20}(t) \quad (14)$$

In addition, the initial conditions that need to be specified were:

$$t = 0, T_1(x, t) = f_1(x), T_2(x, t) = f_2(x) \quad (15)$$

Here, $T(x, t)$ indicated that T_1 and T_2 were binary functions of x and t now. In Equation (9), the boundary value can be a constant, and in reality it was also a controlled constant.

Equations (12) and (13) formed first-order linear partial differential equations, which were difficult to solve. Considering that the temperature of the fluid in the inner tube varied widely and that of the outer tube varied little, assuming that the temperature of the fluid in the inner tube (T_2) was a constant value, the problem can be reduced to a first-order linear differential equation:

$$S\rho_{h1}c_{p_{h1}}\frac{\partial T_1}{\partial t} + m_{h1}c_{p_{h1}}\frac{\partial T_1}{\partial x} = K\pi DT_{20} - K\pi DT_1 \quad (16)$$

The boundary conditions and initial conditions were:

$$x = 0, T_1 = T_{10} \quad (17)$$

$$t = 0, T_1(x, t) = f_1(x) = T_{00} \quad (18)$$

According to Cauchy method [21], the characteristic equations of Equation (16) were:

$$\frac{dt}{ds} = S\rho_{h1}c_{p_{h1}}, \quad \frac{dx}{ds} = m_{h1}c_{p_{h1}}, \quad \frac{du}{ds} = K\pi D(T_{20} - T_1) \quad (19)$$

If the average fluid velocity $v_{h1} = m_{h1}/(S \cdot \rho_{h1})$ was fixed, Equation (20) can be obtained:

$$\frac{dt}{ds} = S\rho_{h1}c_{p_{h1}}, \quad \frac{dx}{ds} = v_{h1}S\rho_{h1}c_{p_{h1}}, \quad \frac{du}{ds} = K\pi D(T_{20} - T_1) \quad (20)$$

and their solutions were:

$$t = S\rho_{h1}c_{p_{h1}}s + C_1 \quad (21)$$

$$x = v_{h1}S\rho_{h1}c_{p_{h1}}s + C_2 \quad (22)$$

$$-\ln(T_{20} - T_1) = K\pi Ds + C_3 \quad (23)$$

s can be eliminated by Equations (21), (23) and (24) was obtained:

$$-\ln(T_{20} - T_1) = \frac{K\pi D}{S\rho_{h1}c_{p_{h1}}}t + C_{31} \quad (24)$$

The constant C_{31} was determined by the initial condition (when $t = 0$, $T = T_{10}$), that was:

$$\frac{T_{20} - T}{T_{20} - T_{00}} = \exp\left(-\frac{K\pi D}{S\rho_{h1}c p_{h1}}t\right), \rightarrow (x > v_{h1}t) \quad (25)$$

s can be eliminated by Equations (22), (23) and (26) was obtained:

$$-\ln(T_{20} - T_1) = \frac{K\pi D}{v_{h1}S\rho_{h1}c p_{h1}}x + C_{32} \quad (26)$$

The constant C_{32} was determined by the boundary condition (when $x = 0$, $T = T_{10}$), that was:

$$\frac{T_{20} - T}{T_{20} - T_{10}} = \exp\left(-\frac{K\pi D}{v_{h1}S\rho_{h1}c p_{h1}}x\right), \rightarrow (x < v_{h1}t) \quad (27)$$

s can be eliminated by Equations (21), (22) and (28) was obtained:

$$x = v_{h1}t + C_{12} \quad (28)$$

Equation (28) was the basis for determining the application scope of Equations (25) and (27). Under specific temperature conditions, the corresponding temperature curve results in the heat exchanger can be solved.

3.2. Model and Solution Method of Pyrolysis Steam Coupled Multi-Stage Condensers

From the heat transfer relationship of a single condenser, the condensation characteristics of the internal fluids can be obtained. A single condenser can be connected in series to obtain multi-stage condensers. Each condenser was separately proposed as a heat exchange unit, and only had the input and output of hot (pyrolysis steam) and cold fluids, where the output hot fluid of the previous stage was used as the input hot fluid of the latter stage, and the multi-stage condensers can be simplified and combined. Taking the four-stage condensers as an example, the structure and model are shown in Figure 3.

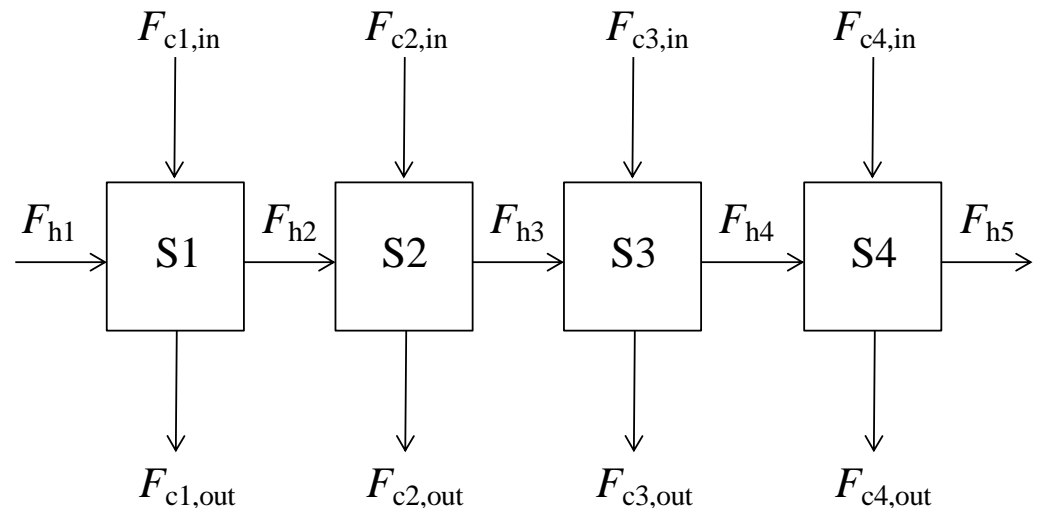


Figure 3. Schematic diagram of the multi-stage condensers model.

Therefore, the key was to reasonably establish the relationship between the output fluid parameters of each stage and all external input fluid parameters before this stage. In actual operation, the mass flow rate and temperature of the input hot fluid $F_{h1,in}$ and the input cold fluids $F_{c1,in}$, $F_{c2,in}$, $F_{c3,in}$, and $F_{c4,in}$ of each stage condenser were fixed values. When the structure parameters of the condensers were determined, the mass flow rates and temperatures of the output hot fluid $F_{h1,out}$ ($F_{h2,in}$), $F_{h2,out}$ ($F_{h3,in}$), and $F_{h3,out}$ ($F_{h4,in}$), and the final output fluid $F_{h4,out}$ (F_{h5}) were only related to the input parameters.

In the actual experiment process, after biomass (larch was selected in this study) particles were pyrolyzed at 550 °C and gas–solid separation, the temperature of the pyrolysis steam entering the multi-stage condensers can be assumed to be 400 °C [22] and the main physical properties of the composition of the pyrolysis steam at the qualitative temperature are shown in Table 3 [11]. The weighted averages of the components of the above pyrolysis steam are calculated to obtain the model compound that entered the first-stage condenser, as shown in Table 4. The thermodynamic calculation of the first-stage condenser can be performed, and then the outlet temperature of the hot fluid was obtained. The composition of the pyrolysis steam at this temperature and its respective main physical properties [23] were checked and obtained, and a weighted average was performed to obtain a new model compound. Then, the hot fluid entering the second-stage condenser can be obtained, and the thermodynamic calculation of the second-stage condenser can also be performed, which was similar to that of the third and fourth-stage condensers.

Table 3. Composition of Pyrolysis Steam Produced from Larch and The Physical Properties.

Compound	Content, %	Physical Properties at the Qualitative Temperature			
		Specific Heat Capacity, kJ/(kg·°C)	Density, kg/m ³	Dynamic Viscosity, 10 ^{−5} Pa·s	Thermal Conductivity, W/(m·°C)
Acetic acid	16.67	2.176	0.398	0.016	0.048
Ethyl acetate	5.76	1.943	0.143	1.731	0.049
Resorcinol	4.93	2.559	0.427	1.278	0.031
2,5-diethoxy tetrahydrofuran	2.52	1.879	0.212	0.015	0.039
7-hydroxy-3-Methylcyclopent-7-enone	2.02	2.438	0.268	0.012	0.034
7-methoxyphenyl acetate	1.99	3.311	0.166	0.015	0.044
4-propenyl-7-methoxyphenol	1.82	2.252	0.145	0.019	0.032
4-hydroxy-7-methoxybenzaldehyde	6.74	1.781	0.181	0.016	0.061
Catechol	5.84	3.933	0.242	0.013	0.035
Furan aldehyde	4.93	1.344	0.221	0.019	0.065
3-methoxybenzaldehyde	2.77	3.801	0.187	0.014	0.043
Phenol	2.54	1.943	0.455	0.016	0.041
7-methoxy-4-methyl phenol	1.84	1.478	0.153	1.514	0.039
Water	38.31	3.715	0.912	0.054	0.062

Table 4. Model Compound (Hot Fluid) Properties of the First-Stage Condenser at the Qualitative Temperature.

Specific Heat Capacity, kJ/(kg·°C)	Density, kg/m ³	Dynamic Viscosity, 10 ^{−5} Pa·s	Thermal Conductivity, W/(m·°C)
2.883	0.529	0.249	0.053

4. Numerical Simulation

4.1. Scheme Comparison

First, the first-stage condenser was taken as an example, the mathematical models of the four schemes were solved separately, and the basic thermodynamic characteristics

were obtained and analyzed. The $m_{h1} = 3 \times 10^{-3}$ kg/s, $T_1 = 400$ °C, and $T_2 = 80$ °C were retained and the changing trends of the hot fluid outlet temperature and thermal load in the dual tube heat exchanger with the mass flow rate of the cold fluid are shown in Figure 4. Figure 4a shows the comparison of the hot fluid outlet temperatures. It can be seen that as m_{c1} increased, the hot fluid outlet temperature gradually decreased, and it was the lowest and the declined most rapidly in Scheme 1. The heat exchange of the cold and hot fluids in Scheme 4 was the worst, indicating that placing the hot fluid in the inner tube of the condenser can achieve more sufficient heat exchange. It was worth noting that, compared with Scheme 2, the hot fluid outlet temperature in Scheme 3 was lower, indicating that when the hot and cold fluids flowed countercurrently (the flow directions of the cold and hot fluids were opposite), the heat exchange was better than that of the cocurrent flow (the flow directions of the cold and hot fluids were the same), because the average temperature difference of the countercurrent heat exchange was larger. Figure 4b compares the thermal load of the four schemes, and the thermal load referred to the total energy of heat transfer. It can be seen that as m_{c1} increased, the thermal load in Scheme 1 was higher and the increasing trend was greater, which also showed that it was more sensitive to m_{c1} and the adjustable range was larger. The thermal load in Scheme 3 was higher than Scheme 2, which showed again that the countercurrent heat transfer effect was better. In summary, Scheme 1 was more suitable for realizing highly efficient heat exchange between cold and hot fluids.

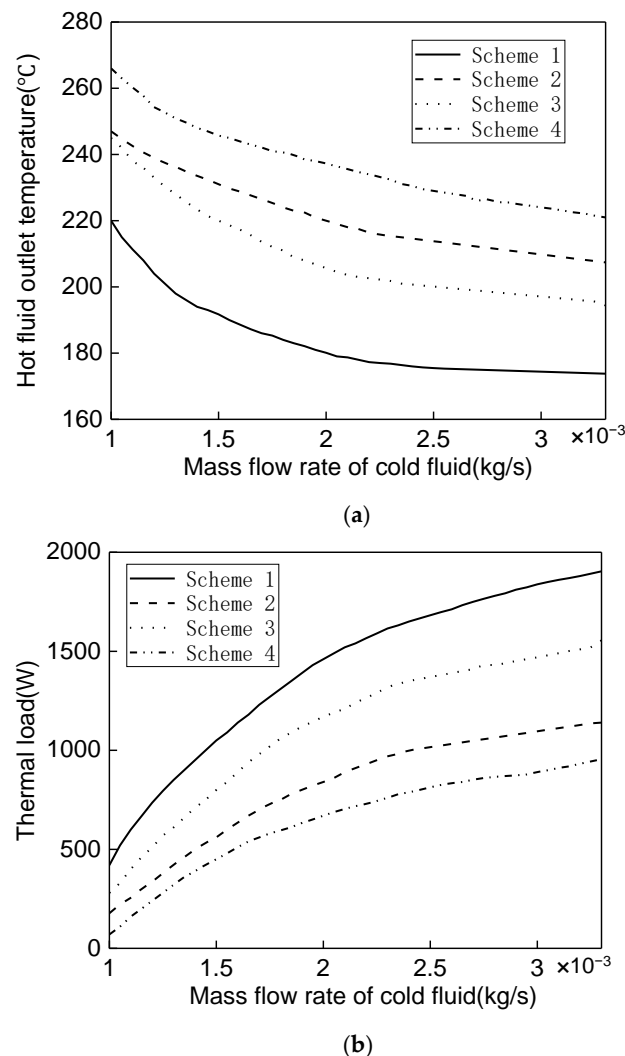


Figure 4. Comparison of the thermodynamic characteristics of the four convective heat transfer schemes ((a) fluid temperature distribution; (b) thermal load).

4.2. Thermodynamic Characteristics

To determine the most suitable number of condensation stages, refer to the commonly used stages in the existing literature [24–26], connecting three, four, five, and six condensers in series. The $m_{h1} = 3 \times 10^{-3}$ kg/s, $T_{h1,in} = 400$ °C, $T_{c1,in} = 80$ °C, $T_{c2,in} = 70$ °C, $T_{c3,in} = 50$ °C, $T_{c4,in} = 30$ °C, $T_{c5,in} = 20$ °C, $T_{c6,in} = 10$ °C, and m_c in each condenser remained the same, the hot fluid outlet temperature and the thermal load changes at the last stage of the condenser with m_c were obtained at different condensation stages, as shown in Figure 5. It can be seen that as m_c and the number of condensation stages increased, the hot fluid outlet temperature and thermal load of the final stage in the multi-stage condensers decreased and increased, respectively. At the same time, when the four, five, and six condensers were connected in series, the difference in the hot fluid outlet temperature and thermal load of the last stage was very small, and the system achieved sufficient heat exchange. Continuing to connect condensers in series can basically not have a greater impact on the overall thermodynamic characteristics, illustrating that when the number of condensation stages reached four, the thermodynamics of the system achieved dynamic equilibrium, so the four-stage condensers in series were selected as the final scheme.

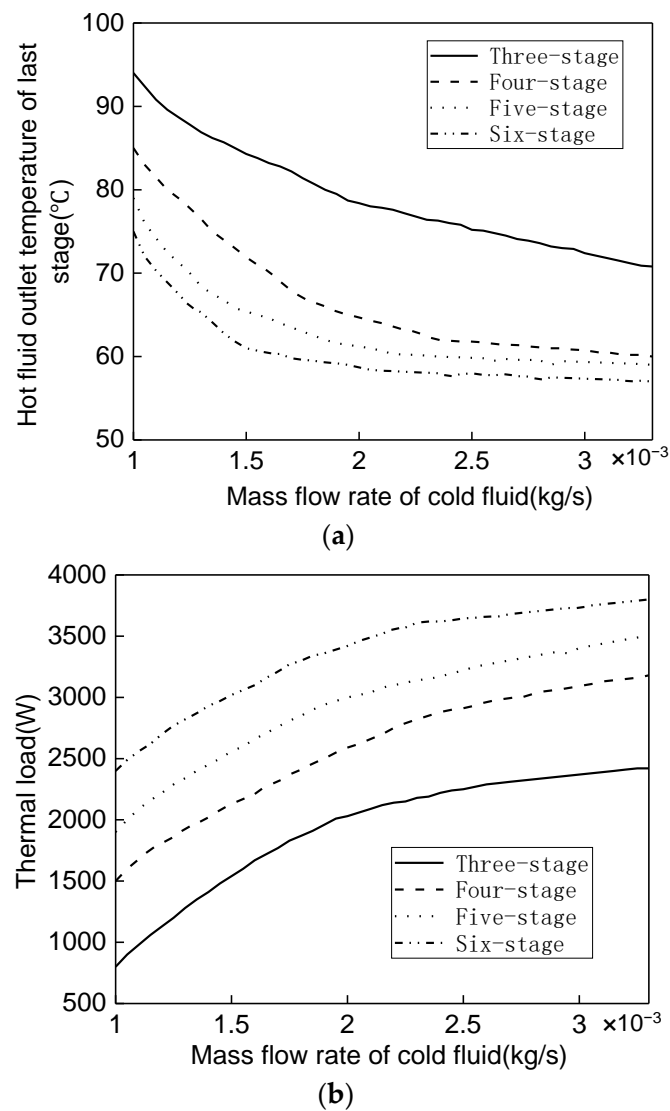


Figure 5. Comparison of the thermodynamic characteristics of the different numbers of condensers ((a): outlet temperature; (b): thermal load).

Similarly, keeping $m_{h1} = 3 \times 10^{-3}$ kg/s, $T_{h1,in} = 400$ °C, $T_{c1,in} = 80$ °C, $T_{c2,in} = 70$ °C, $T_{c3,in} = 50$ °C, $T_{c4,in} = 30$ °C, and m_c in each condenser the same, the relationship of the overall heat transfer coefficient in each condenser and mass flow rate of cold fluid of the four-stage condensers was obtained, as shown in Figure 6. It can be seen that the overall heat transfer coefficient of the first-stage condenser was the largest, and as the number of condensation stages increased, the overall heat transfer coefficient decreased successively, indicating that the heat exchange of the hot and cold fluids mainly occurred in the first-stage condenser, and even if m_c of the subsequent condensers increased, its overall heat transfer coefficient cannot increase significantly, indicating that the heat transfer process reached saturation. At the same time, it showed that the four-stage condensers in series completely realized the heat exchange of hot and cold fluids.

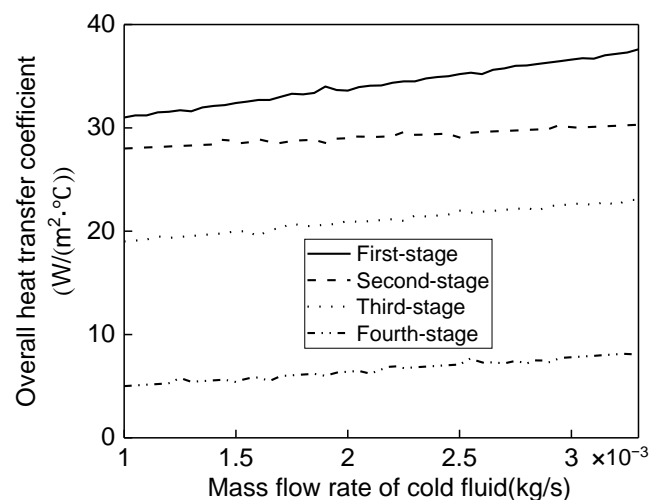


Figure 6. Comparison of the overall heat transfer coefficients of each stage of the four-stage condensers.

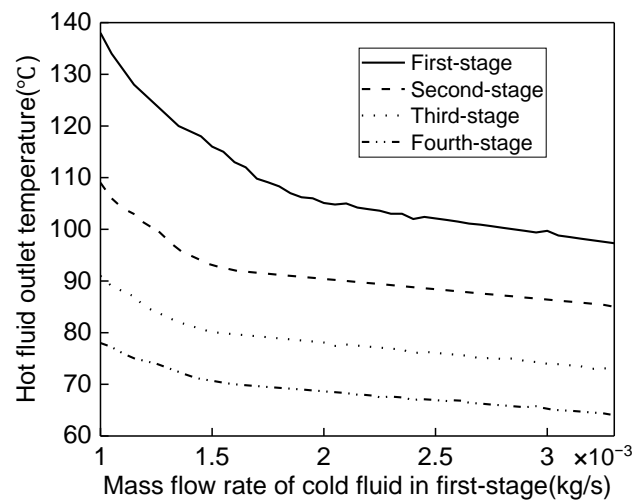
4.3. Operation Characteristics

Next, the regulating characteristics of the four-stage condensers were studied to evaluate the operation characteristics of the entire condensers system. It can be seen from the above results that the mass flow rate of the cold fluid had a significant impact on the heat transfer effect of the condenser. In order to further explore the behavior of the mass flow rate of the cold fluid at each condenser level on the thermodynamics of the system, the changing trends of the hot fluid outlet temperature and thermal load were investigated.

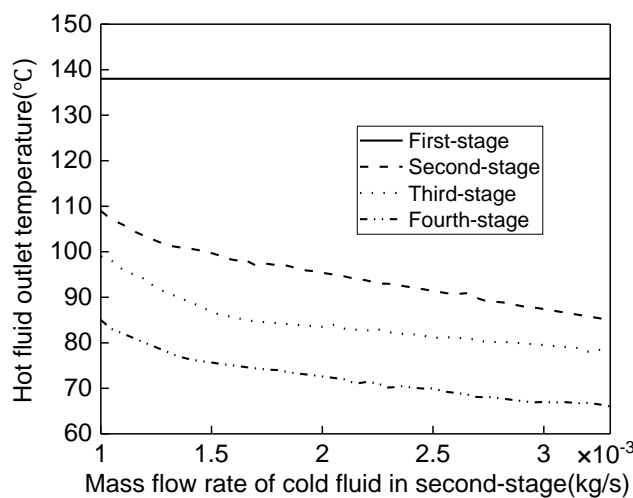
Similarly, keeping $m_{h1} = 3 \times 10^{-3}$ kg/s, $T_{h1,in} = 400$ °C, $T_{c1,in} = 80$ °C, $T_{c2,in} = 50$ °C, $T_{c3,in} = 30$ °C, and $T_{c4,in} = 10$ °C the same, only the mass flow rate of cold fluid in the one-stage condenser was changed, while other three condensers remained at 1×10^{-3} kg/s, and the regulating relationship between the hot fluid outlet temperature and the mass flow rate of the cold fluid of each condenser in the four-stage condensers was obtained, as shown in Figure 7. In Figure 7a, as m_{c1} increased, the hot fluid outlet temperature at each stage condenser dropped rapidly and then slowly, and the temperature changes in the subsequent three-stage condensers gradually decreased, even the changing trend of the temperature curve of the fourth-stage condenser was close to linear. In Figure 7b, when m_{c2} changed, the hot fluid outlet temperature in the first-stage condenser remained unchanged, and the hot fluid outlet temperature of the subsequent three-stage condensers also dropped rapidly and then slowly. However, the changing magnitude of the curve was significantly lower than that in Figure 7a, and when the mass flow rates of the cold fluid in the first- and second-stage condensers were the same, the hot fluid outlet temperatures were much higher. Figure 7c,d is the same as the above two figures. The above results indicated that in order to quickly reduce the hot fluid outlet temperature, the key was to increase the mass flow rate of the cold fluid in the first-stage condenser, quickly realize the heat exchange between the cold and hot fluids and increase the mass flow rates of the

cold fluid in the subsequent condensers; even if they increased a lot, the hot fluid outlet temperature may still be higher.

At the same time, in the same operation conditions, the regulating relationship between the thermal load and the mass flow rate of the cold fluid of each condenser in the four-stage condensers was obtained, as shown in Figure 8. In Figure 8a, as m_{c1} increased, the thermal load of each condenser gradually increased, and the thermal load of the first-stage condenser changed the most. The reason was that the temperature difference between the cold and hot fluids in the first-stage condenser was the largest, and the total heat exchange was also the largest. In Figure 8b, as m_{c1} increased, the thermal load of the first-stage condenser remained unchanged, and the changing trend of the thermal loads of the subsequent three-stage condensers were the same, but the amplitudes were significantly lower. The reason was that although the mass flow rate of the cold fluid in the first-stage condenser was low, the hot fluid temperature still dropped, resulting in a decrease in the subsequent thermal load. Figure 8c,d is the same as the above two figures. This phenomenon also illustrated the importance of the first-stage condenser for the heat transfer efficiency of the entire system.

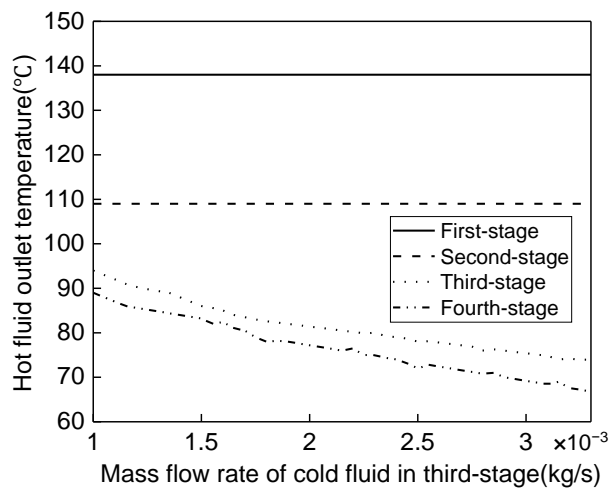


(a)

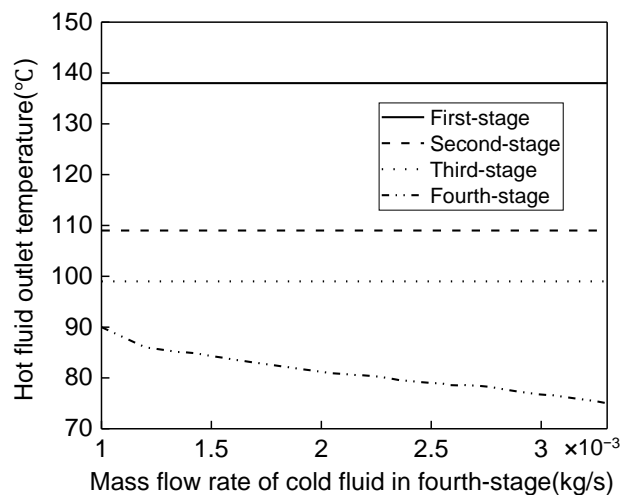


(b)

Figure 7. Cont.

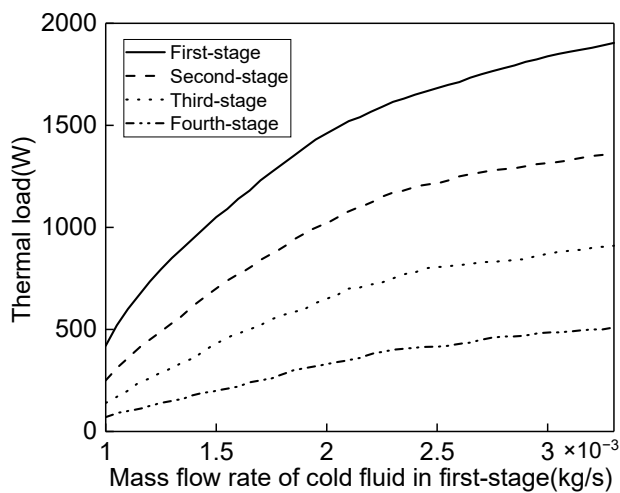


(c)



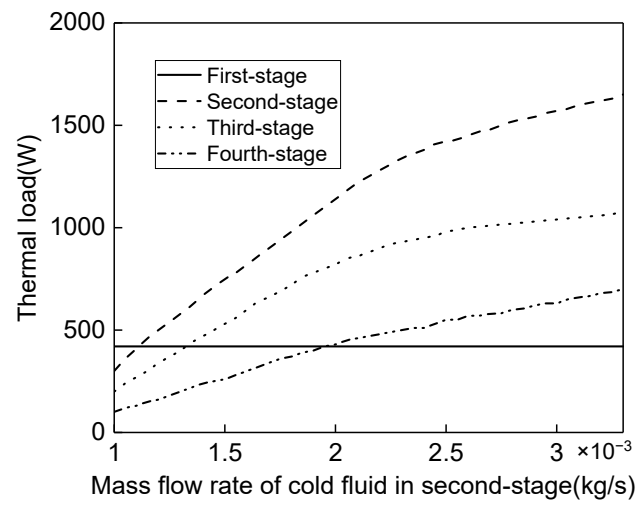
(d)

Figure 7. Regulating relationships between the output hot fluid temperature and mass flow rate of the cold fluid in each condenser.

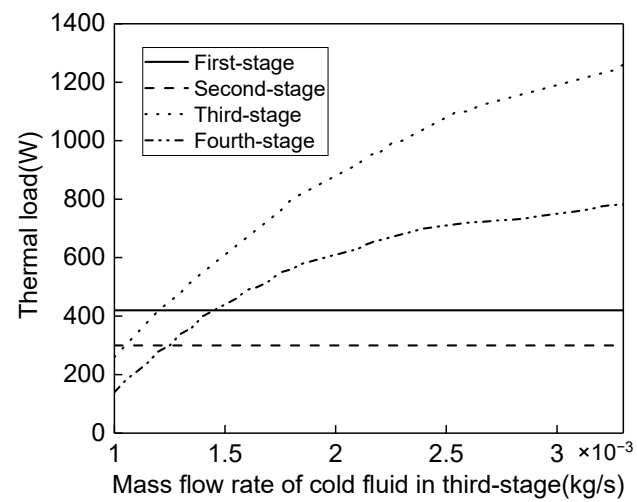


(a)

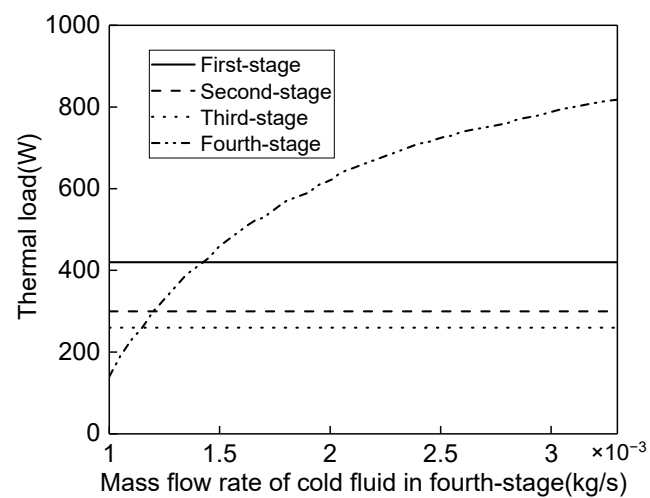
Figure 8. Cont.



(b)



(c)



(d)

Figure 8. Regulating relationships between thermal load and mass flow rate of cold fluid in each condenser.

5. Experimental Verification

5.1. Apparatus and Method

To verify the above theoretical calculation conclusions, the pyrolysis steam coupled four-stage condensers experimental apparatus was set up, as shown in Figure 9. The high-temperature pyrolysis steam (400 °C) produced by the pyrolysis reactor entered the first-stage condenser after gas–solid separation. When the heat exchange was completed, the ball valve at the bottom of the condenser was opened to collect the condensed products, and the remaining gas entered the second-stage condenser for the second heat exchange, and so on. Finally, the non-condensable gas was discharged after four heat exchanges. The four-stage condensers were equipped with heaters to heat the cold fluids in the water tanks at 80, 50, 30, and 10 °C, and the mass flow rate varied from $1\sim 3 \times 10^{-3}$ kg/s. The thermometers were used to monitor the temperature of the cold fluid to adjust the heater power. The flowmeters on the cold fluid pipelines were used to measure the mass flow rate, and the ball valves were used to relieve the pressure to ensure the safety of the system.

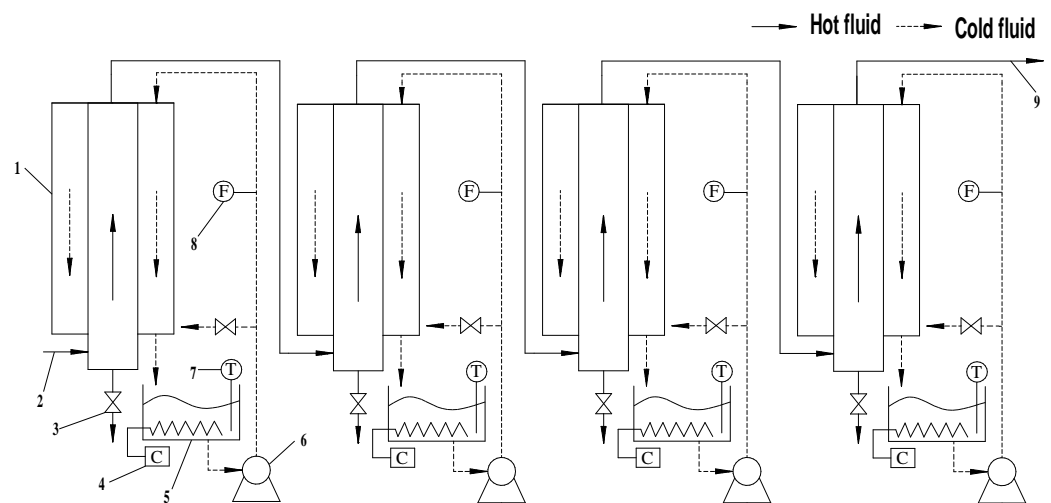


Figure 9. Schematic diagram of the four-stage condensers experimental apparatus for thermodynamic characteristics: (1) dual tube heat exchanger; (2) pyrolysis steam inlet; (3) ball valve; (4) heater; (5) water tank; (6) circulation pump; (7) thermometer; (8) rotor flow meter; (9) non-condensable gas outlet.

The purpose of the experiment was to set the mass flow rate and temperature of the cold fluid, measure and calculate the hot fluid outlet temperature of the final stage condenser and the yield of the collected liquid product of each condenser, and compare them with the theoretical calculation results. To facilitate the operation, the mass flow rate and temperature of pyrolysis steam were kept constant, and only the mass flow rates of the cold fluids were changed.

5.2. Results and Discussion

The hot fluid outlet temperature of the final stage at different cold fluid mass flow rates was measured experimentally, and compared with the calculated results, as shown in Figure 10. It can be seen that as the mass flow rate of the cold fluid increased the calculated values and the measured values were in good agreement, and the maximum deviation did not exceed 10%. The reason may be that the hot and cold fluids had more heat exchange with the outside environment during the actual experiment, and the thermal preservation was insufficient.

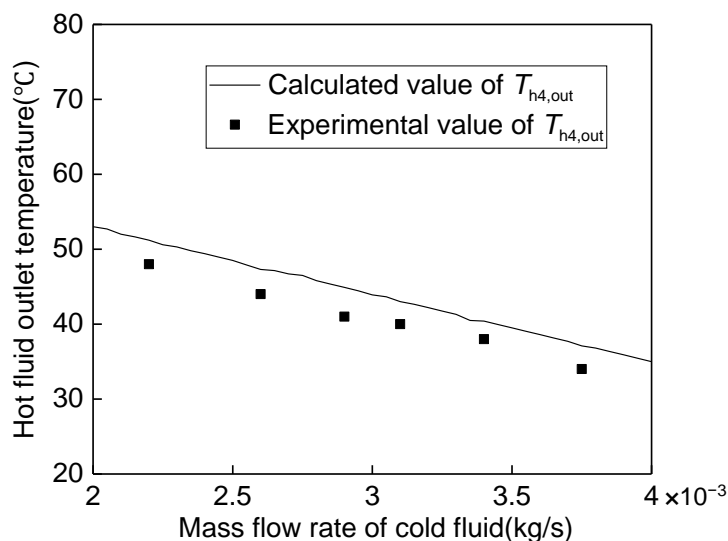


Figure 10. Experimental verification of the hot fluid outlet temperature of the four-stage condensers.

At the same time, when the mass flow rate of the cold fluid of each stage condenser was 3×10^{-3} kg/s, the yield range of the liquid product of each stage condenser was obtained, as shown in Figure 11. It can be seen that the yield of the first-stage condenser was the highest and had the largest fluctuation range and yields of the subsequent condensers decreased sequentially. The reason was also that the first-stage condenser, as the main place for the heat exchange of hot and cold fluids, must have the most condensed products. The gradual decrease in the fluctuation range was likely to be caused by the liquefaction of water steam. The above results demonstrated the importance of the first-stage condenser, and its liquid product yield was higher than the literature results [12,27].

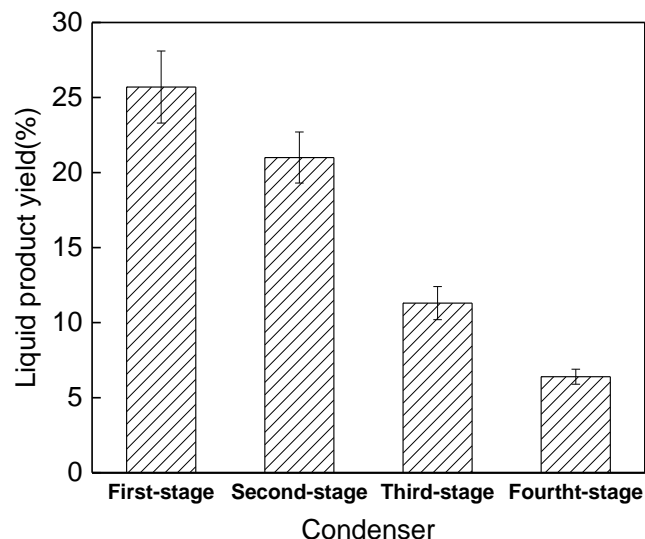


Figure 11. The liquid product yield collected by each condenser of the four-stage condensers.

6. Conclusions

The multi-stage condensers, where the pyrolysis steam and water conducted countercurrent convective heat exchange, were designed to facilitate staged condensation and recovery of pyrolysis oil. The single condenser model was established for the discipline of the heat transfer between the internal fluids. Then, the model of the pyrolysis steam coupled multi-stage condensers was proposed to study the effect of the mass flow rate of cold fluid of each condenser on the thermodynamic characteristics of the entire system.

Finally, this developed model was verified experimentally, indicating that it was highly rational. The main conclusions were as follows:

- (1) According to the flow direction of the cold and hot fluids, and the structural characteristics of the dual tube heat exchanger, four condensation schemes of pyrolysis steam convective heat exchange were proposed to achieve rapid condensation and recover liquid products.
- (2) The single condenser models of the four schemes were established. Based on the control micro-element, the heat transfer disciplines of the internal fluids were obtained with the help of the heat transfer differential equation. The numerical simulation results showed that the convective heat transfer effect of the cold and hot fluids in Scheme 1 was best. At the same time, with the help of the concept of the model compound, the pyrolysis steam coupled multi-stage condensers model was proposed. The thermodynamic characteristics of with four different numbers of the condensers in series were also simulated. The results showed that when the number of condensers in series was four, the heat transfer process of the system reached saturation, and the heat exchange of the cold and hot fluids was completely realized, and it was of little significance to continue to connect more condensers in series for the condensation of pyrolysis steam.
- (3) Further calculations were carried out for the four-stage condensers, and the basic thermodynamic and operation characteristics were obtained. The results showed that in order to quickly reduce the hot fluid outlet temperature, the key was to increase the mass flow rate of the cold fluid in the first-stage condenser. While the mass flow rates of the cold fluid in the subsequent condensers increased a lot, the hot fluid outlet temperature may still be higher. The first-stage condenser was critical to the heat transfer efficiency of the entire system.
- (4) The four-stage condensers experimental apparatus was set up and experimental verification was carried out. The results showed that the calculated values obtained by the developed model were in good agreement with the measured values, and the deviation did not exceed 10%, better than the results of the literature [12,27]. At the same time, the liquid product yields of each condenser at the fixed conditions were obtained, which also showed the importance of the first-stage condenser.

A possible future research focus: we need to focus on analyzing the purity of the products obtained by each condenser, infer the pros and cons of their respective condensing states, to provide more guidance for the selection of actual operating parameters.

Author Contributions: Conceptualization, Y.B. and Y.M.; methodology, Y.B.; software, Y.B.; validation, Y.B., C.K. and W.C.; formal analysis, Y.B. and G.G.; investigation, Y.B. and P.Z.; resources, Y.B. and C.C.; data curation, Y.B. and L.L.; writing—original draft preparation, Y.B. and X.Y.; writing—review and editing, Y.B. and Y.M.; visualization, Y.B. and Z.F.; supervision, Y.B. and Y.M.; project administration, Y.B.; funding acquisition, Y.M. All authors have read and agreed to the published version of the manuscript.

Funding: This research was supported by the fund of the Youth Innovation Promotion Association, CAS, NO.Y2021048, Research Group of Short Pulse Laser Technology of Chinese Academy of Sciences, Condition Guarantee and Finance Department (No.GJJSTD20200009).

Institutional Review Board Statement: Not applicable.

Informed Consent Statement: Not applicable.

Data Availability Statement: The study did not report any data.

Acknowledgments: All workers are acknowledged. The writers also acknowledge the assistance of the anonymous reviewers.

Conflicts of Interest: The authors declare no conflict of interest.

Nomenclature

Symbols

F	fluid
$cp_{c1,in}$	average constant pressure specific heat capacity of the fluid in the outer tube, $\text{kJ}/(\text{kg}\cdot^{\circ}\text{C})$
cp_{h1}	average constant pressure specific heat capacity of the fluid in the inner tube, $\text{kJ}/(\text{kg}\cdot^{\circ}\text{C})$
D	diameter of the inner tube, m
K	overall heat transfer coefficient, $\text{W}/(\text{m}^2\cdot^{\circ}\text{C})$
$m_{c1,in}$	mass flow rate of fluid in the outer tube, kg/s
m_{h1}	mass flow rate of fluid in the inner tube, kg/s
S	cross-sectional area of the inner tube, m^2
T	temperature, $^{\circ}\text{C}$
t	time, s
v	average fluid velocity, m/s
Δq	thermal energy of the micro-element section, J
Δx	length of the micro-element section, J

Greek Letters

ρ	density, kg/m^3
--------	---------------------------------

Subscripts

c	cold fluid
hot	hot fluid
in	parameters of the fluid inlet
out	parameters of the fluid outlet
1	first-stage condenser

References

- Zhang, Z.Y.; Ju, R.; Zhou, H.T.; Chen, H.W. Migration characteristics of heavy metals during sludge pyrolysis. *Waste Manag.* **2021**, *120*, 25–32. [[CrossRef](#)] [[PubMed](#)]
- Bai, Y.; Si, H. Experimental study on feeding characteristics of conical bottom pneumatic spout feeder for biomass pyrolysis. *Chem. Eng. Process.* **2021**, *166*, 108490. [[CrossRef](#)]
- Koshelev, M.M.; Ulyanov, V.V.; Kharchuk, S.E. Study of the Fractional Composition of Liquid Products of Pyrolysis of Solid Organic Waste in Liquid Lead. *Theor. Found. Chem. Eng.* **2021**, *55*, 671–676. [[CrossRef](#)]
- Bai, Y.; Liu, D.C.; Si, H. A three-stage heating system of dual-fuel controlled by negative feedback for fluidized bed fast pyrolysis. *Sustain. Energy Technol.* **2021**, *46*, 101228. [[CrossRef](#)]
- Liu, L.S.; Zhang, X.Y.; Zhao, R.X.; Song, G.J.; Tian, L. Pyrolysis of Phragmites hirsuta study on pyrolysis characteristics, kinetic and thermodynamic analyses. *Int. J. Energ. Res.* **2021**, *45*, 15200–15216. [[CrossRef](#)]
- Gulec, F.; Simsek, E.H.; Sari, H.T. Prediction of Biomass Pyrolysis Mechanisms and Kinetics: Application of the Kalman Filter. *Chem. Eng. Technol.* **2021**, *45*, 167–177. [[CrossRef](#)]
- Bai, Y.; Qi, J.Y.; Si, H. Analytical study on the Heat-Transfer Characteristics of a Fluidized Bed Reactor Heated by Multi-Stage Resistance. *Chem. Eng. Process.* **2021**, *164*, 108395. [[CrossRef](#)]
- Song, Y.; Liang, H.B.; Chen, Z.X.; Ma, J. Mechanism of Low Temperature Pyrolysis of Oily Sludge A Case Study of Daqing Oilfield CHINA. *Fresenius Environ. Bull.* **2021**, *30*, 5954–5960.
- Tuntsev, D.V.; Shaikhutdinova, A.R. Mathematical description of the process of condensation of pyrolysis fuel during fast pyrolysis of woody biomass. *Energy Source Part A* **2020**, *42*, 1599–1607. [[CrossRef](#)]
- Zhu, X.F.; Luo, Z.J.; Zhu, X.F. Novel insights into the enrichment of phenols from walnut shell pyrolysis loop: Torrefaction coupled fractional condensation. *Waste Manag.* **2021**, *131*, 462–470. [[CrossRef](#)] [[PubMed](#)]
- Zhang, Z.; Macquarrie, D.J.; De Bruyn, M.; Budarin, V.L.; Hunt, A.J.; Gronnow, M.J.; Fan, J.; Shuttleworth, P.S.; Clark, J.H.; Matharu, A.S. Low-temperature microwave-assisted pyrolysis of waste office paper and the application of bio-oil as an Al adhesive. *Green Chem.* **2021**, *131*, 462–470. [[CrossRef](#)]
- Wang, J.X.; Zhang, S.P.; Chen, M.Z.; Feng, Y.H.; Zhang, H.Y. Fractional condensation of pyrolysis oil from fast pyrolysis of food waste digestate for enrichment of high value-added nitrogen-containing components. *J. Anal. Appl. Pyrol.* **2022**, *166*, 105609. [[CrossRef](#)]
- Gooty, A.T. *Fractional Condensation of Bio-Oil Vapors*; The University of Western Ontario: London, ON, Canada, 2013.
- Lei, Z.; Hao, S.; Lei, Z.; Yang, J. Gas-Modified Pyrolysis Coke for in Situ Catalytic Cracking of Coal Tar. *ACS Omega* **2020**, *5*, 14911–14923. [[CrossRef](#)]
- Upham, D.C.; Agarwal, V.; Khechfe, A.; Snodgrass, Z.R.; Gordon, M.J.; Metiu, H.; McFarland, E.W. Catalytic molten metals for the direct conversion of methane to hydrogen and separable carbon. *Science* **2017**, *358*, 917–920. [[CrossRef](#)] [[PubMed](#)]

16. Anderson, E.M.; Stone, M.L.; Katahira, R.; Reed, M.; Beckham, G.T.; Roman-Leshkov, Y. Flowthrough Reductive Catalytic Fractionation of Biomass. *Joule* **2017**, *1*, 613–622. [[CrossRef](#)]
17. Li, N.; Fan, X.D.; Wang, X.Y.; Deng, H.; Zhang, K.; Zhang, X.G.; Han, Q.Y.; Lv, Y.; Liu, Z.W. Autophagy-Related 5 Gene rs510432 Polymorphism Is Associated with Hepatocellular Carcinoma in Patients with Chronic Hepatitis B Virus Infection. *Immunol. Investig.* **2019**, *48*, 378–391. [[CrossRef](#)] [[PubMed](#)]
18. Sakakibara, H.; Usui, H.; Suzuki, K.; Kotani, T.; Aoki, H.; Kuroki, K. Model Construction and a Possibility of Cupratelike Pairing in a New d(9) Nickelate Superconductor (Nd, Sr)NiO₂. *Phys. Rev. Lett.* **2020**, *125*, 077003. [[CrossRef](#)]
19. Heidari, M.; Dutta, A.; Acharya, B.; Mahmud, S. A review of the current knowledge and challenges of hydrothermal carbonization for biomass conversion. *J. Energy Inst.* **2019**, *92*, 1779–1799. [[CrossRef](#)]
20. Belbessai, S.; Azara, A.; Abatzoglou, N. Recent Advances in the Decontamination and Upgrading of Waste Plastic Pyrolysis Products: An Overview. *Processes* **2022**, *10*, 733. [[CrossRef](#)]
21. Liu, T.B.; Qin, X.W.; Li, Q.Y. An optimal fourth-order family of modified Cauchy methods for finding solutions of nonlinear equations and their dynamical behavior. *Open Math.* **2019**, *17*, 1567–1598. [[CrossRef](#)]
22. Bridgwater, A.V.; Peacocke, G.V.C. Fast pyrolysis processes for biomass. *Renew. Sustain. Energy Rev.* **2000**, *4*, 1–73. [[CrossRef](#)]
23. Zi, Z.W. *Petrochemical Design Manual*; Chemical Industry Press: Beijing, China, 2015. (In Chinese)
24. Jeng, J.S.; Wu, C.M. Fabrication of solution-processed nitrogen-doped niobium zinc tin oxide thin film transistors using ethanolamine additives. *J. Alloy Compd.* **2017**, *729*, 370–378. [[CrossRef](#)]
25. Quan, H.Y.; Wang, L.Y.; Wang, Z.N.; Mei, X.D.; Ning, J.; She, D.M. Application of N-Acylimidazoles in the Claisen Condensation Reaction. *ChemistrySelect* **2020**, *5*, 7222–7226. [[CrossRef](#)]
26. Li, X.Y.; Lin, B.N.; Li, H.B.; Yu, Q.; Ge, Y.; Jin, X.; Liu, X.H.; Zhou, Y.H.; Xiao, J.P. Carbon doped hexagonal BN as a highly efficient metal-free base catalyst for Knoevenagel condensation reaction. *Appl. Catal. B Environ.* **2018**, *239*, 254–259. [[CrossRef](#)]
27. Li, C.; Zhang, C.T.; Hu, X. Biochar catalyzing polymerization of the volatiles from pyrolysis of poplar wood. *Int. J. Energy Res.* **2021**, *45*, 13936–13951. [[CrossRef](#)]